

High-Visibility Multi-Photon Interference of Classical Light

I. N. Agafonov, M. V. Chekhova, T. Sh. Iskhakov, A. N. Penin

*Department of Physics,
M.V.Lomonosov Moscow State University,
Leninskie Gory, 119992 Moscow, Russia*

It is shown that the visibility of multi-photon interference for classical sources grows rapidly with the order of interference. For three-photon and four-photon interference of two coherent sources, the visibility can be as high as 81.9% and 94.4%, respectively, - much higher than the 'classical limit' of two-photon interference (50%). High-visibility three-photon and four-photon interference has been observed in experiment, for both coherent and pseudo-thermal light.

PACS numbers: 42.50.Dv, 03.67.Hk, 42.62.Eh

It is known that the nonclassical phenomena of two-photon interference [1] and two-photon ghost diffraction and imaging [2], [3] have classical counterparts. Two-photon interference of classical light has been first discovered in the pioneering experiments by Hanbury Brown and Twiss [4] and since then was observed with various sources, including pseudo-thermal ones [5], true thermal ones [6], and coherent ones [7]. Somewhat later, ghost imaging with classical light has been demonstrated, both in the near-field and far-field domains [8], [9], [10]. The only disadvantage of classical light with respect to two-photon interference and two-photon ghost imaging, compared to two-photon entangled sources, is the limited visibility, which is always below 50% [12], [13]. On the other hand, in interference and imaging experiments with classical sources the visibility is independent of the intensity, which can therefore be arbitrarily high. Entangled sources, in contrast, should be sufficiently weak to provide high-visibility interference: while the visibility is close to 100% for faint two-photon light, it drops with the increase in the mean number of photons per mode [14], [8].

In this paper we show that classical sources can provide much better visibility if one passes to higher-order intensity correlations. This fact, which has considerable importance for multi-photon imaging and multi-photon lithography, is also remarkable in view of the numerous recent experiments on higher-order correlations and multi-photon interference [15]. Indeed, while in the case of two-photon interference any experiment with the visibility exceeding 50% can be interpreted as non-classical, no such criterion is formulated for higher-order interference. Our results show that for multi-photon interference to be recognized as nonclassical, its visibility should exceed really high values: 81.9% in the three-photon case and 94.4% in the four-photon one. These values are classical visibility limits for three- and four-photon interference, respectively.

For our consideration, we chose the scheme of the two-slit Young's interference experiment [16]. This geometry was used in many experiments on two-photon interference and two-photon ghost imaging [2], [3], [5], [9],

[8], [10]. This time, however, we consider the interference to be registered by three detectors instead of two (Fig.1), each detector measuring the instantaneous intensity and the triple photocount coincidences being counted by a coincidence circuit. This is the standard experimental technique to measure the third-order Glauber's intensity correlation function (ICF) [11]. Let the two sources A, B be classical ones, having the same statistics, the same average intensities, and independently fluctuating phases. The last condition provides the erasure of the first-order interference in the far-field zone. However, a simple calculation shows that the intensity correlation functions will be sensitive to the positions of the detectors. Passing to the normalized third-order correlation function for the detectors placed at points 1, 2, 3,

$$g_{123}^{(3)} \equiv \frac{\langle I_1 I_2 I_3 \rangle}{\langle I_1 \rangle \langle I_2 \rangle \langle I_3 \rangle}, \quad (1)$$

I_j being the instantaneous intensity at point $j = 1, 2, 3$, we obtain that

$$g_{123}^{(3)} = \frac{g^{(3)}}{4} + \frac{g^{(2)}}{2} \left[\frac{3}{2} + \cos\phi_{12} + \cos\phi_{23} + \cos\phi_{13} \right], \quad (2)$$

where $g^{(2)}, g^{(3)}$ are, respectively, the second-order and third-order normalized ICFs for each of the two sources and $\phi_{ij} \equiv \phi_{Ai} - \phi_{Aj} - \phi_{Bi} + \phi_{Bj}$, ϕ_{Sd} being the phase gained by the radiation of source $S = A, B$ on the way to detector $d = 1, 2, 3$.

According to Eq.(2), the maximal visibility is provided by the radiation sources with the minimal ratio of $g^{(3)}/g^{(2)}$. Among the classical sources, this 'visibility limit' is achieved for coherent light and is equal to 81.9%. Thermal radiation gives a lower visibility, 60%, which is still much higher than the corresponding value in the case of two-photon interference (33%).

In our experiment, the third-order Glauber's correlation function was measured through the coincidence counting rate of three detectors (Fig.2). As the radiation source, we used a frequency doubled Q-switched YAG:Nd laser with the wavelength 532 nm, pulse duration 5 ns, and the repetition rate 3 kHz. Instead of two slits, which should be very precisely matched in width to achieve the

maximum visibility of multi-photon interference, a single slit of width 150μ was used, followed by a birefringent crystal (calcite). The crystal split the beam into the ordinary one and the extraordinary one; with the slit and the crystal placed between crossed polarization (Glan) prisms, this configuration was equivalent to two identical slits separated by a distance of 1.3 mm. In the far-field zone, where the interference pattern was formed, the radiation was attenuated using neutral-density filters and fed into a three-arm Hanbury Brown-Twiss interferometer with three photon-counting avalanche diodes and a triple-coincidence circuit. Attenuation was necessary to keep the average number of photocounts per pulse much less than one; otherwise, because of the detectors dead-time effect, the photocount and coincidence rates would be measured incorrectly. Gating of the registration electronic system provided suppression of the dark noise by several orders of magnitude. In order to scan the interference pattern, thick glass plates were placed at the inputs of detectors 1 and 3. Spatial mode selection was provided by 70μ apertures A1, A2, A3 placed in front of each detector. By turning the glass plates, one could scan the phase of either one or two detectors within the range $0\dots6\pi$. The phase of detector 2 could be adjusted by moving the aperture A2.

The varying relative phase of the two sources was introduced by inserting an electro-optical modulator (EOM) after the calcite crystal. The EOM was oriented in such a way that its bias voltage induced a phase shift between the ordinary and extraordinary beams. Applying an AC voltage with the amplitude 85 V (slightly below the quarter-wave one) and the frequency 50 Hz, we erased the interference pattern in the time-averaged intensity distribution. Although this harmonic phase modulation was different from a randomly varying relative phase of sources *A, B* (Fig.1), it resulted in the same time-averaged ICFs.

We studied third-order interference both for coherent and pseudo-thermal radiation at the input. Pseudo-thermal light was prepared by means of a rotating ground-glass disc placed after the calcite crystal. The envelope of the third-order spatial ICF was determined by the coherence radius of the radiation, which, in its turn, depended on the sizes of the spots formed on the disc by the ordinary and extraordinary beams, and its FWHM corresponded to approximately two periods of the interference pattern. Because of this, the visibility in the case of thermal light was considerably less than the theoretical value.

The results for the coherent and pseudo-thermal cases are presented in Fig.3 a,b, respectively. Experimental points correspond to the normalized third-order Glauber's ICF; curves show the dependencies given by Eq.(2). In Fig.3b, the finite value of the coherence radius was also taken into account. From Eq.(2) one can see that the maximum visibility is achieved when two of

the three phases are varied simultaneously in the opposite directions, $\phi_{12} = -\phi_{32}$. In accordance with this, in our experiment the glass plates in front of detectors 1 and 3 were rotated synchronously, both clockwise (since detector 1 was in the reflected beam and detector 3 in the transmitted beam, this led to the opposite variation of the phases). The obtained visibility for the case of coherent radiation is 74%; for the case of pseudo-thermal radiation, 38%. In each plot, we also show the spatial dependence of single counts for one of the detectors whose phase was scanned. Although the dependence is not completely flat (the variation is caused by the speckle structure of the laser light and the envelope of the single-slit diffraction pattern), the two-slit interference pattern in the intensity distribution is erased. Note that the presented ICF was normalized to the product of the three intensities; as a result, the 'noisy' structure of single-photon counts did not influence the third-order interference pattern.

If the third-order interference pattern is scanned by only one of the three detectors, the visibility is lower than 81.9% but still considerably higher than in the case of the second-order interference. It reaches its maximal value $\frac{\sqrt{2}}{2}$ (approximately 70.5%) when the relative phase between the remaining two detectors is equal to $\pi/2$.

Quite similarly, one can show that the fourth-order intensity interference of two classical sources is given by the formula

$$g_{1234}^{(4)} = \frac{g^{(4)}}{8} + \frac{g^{(3)}}{2} + \frac{3[g^{(2)}]^2}{8} + \frac{g^{(3)} + [g^{(2)}]^2}{4} [\cos \phi_{12} + \cos \phi_{13} + \cos \phi_{14} + \cos(\phi_{12} - \phi_{13}) + \cos(\phi_{12} - \phi_{14}) + \cos(\phi_{13} - \phi_{14})] + \frac{[g^{(2)}]^2}{8} [\cos(\phi_{12} + \phi_{13} - \phi_{14}) + \cos(\phi_{12} + \phi_{14} - \phi_{13}) + \cos(\phi_{13} + \phi_{14} - \phi_{12})]. \quad (3)$$

Here, the same notation for the phases and normalized ICFs is used as in Eq.(2). Analysis of this expression shows that the maximal visibility of the fourth-order interference for thermal sources is 77.8% while for coherent sources, it is 94.4%. The last figure exceeds the visibility values achieved in nearly all known 'four-photon' experiments.

Experimental observation of the fourth-order interference by registering four-fold coincidences was difficult because of the low coincidence counting rate in this case. For this reason, we turned to another method of measuring spatial ICFs, the one based on digital image processing (see, for instance, Ref. [17]). The interference pattern in the far-field zone was registered by a digital photographic camera Canon PowerShot S2 IS. The source, again a frequency-doubled YAG:Nd laser, in this case had a repetition rate 50 Hz. Each frame was made with a single laser pulse, the exposure time (1/60 s) being less than the distance between the pulses. A typical

interference pattern recorded in one frame is shown in Fig.4. To accumulate sufficient statistics, $n = 500$ shots were made. Due to the phase shift introduced by the EOM, the phase of the interference pattern varied from frame to frame, so that the intensity spatial distribution averaged over all frames revealed almost no interference (the visibility of Young's interference pattern was less than 10%). In each frame, a rectangular area was selected, with the dimensions 50 pixels in the vertical (y) direction and 600 pixels in the horizontal (x) direction (a rectangle shown in Fig.4). First, the intensity distribution recorded in each frame was averaged over the y side of the rectangle, so that intensity distributions $I_j(x)$ for all n pulses were obtained. Next, averaging over j was performed, the averaged intensity distribution and the third- and fourth-order normalized correlation functions being calculated as

$$I(x) = \langle I_j(x) \rangle \equiv \frac{1}{n} \sum_{j=1}^n I_j(x), \quad (4)$$

$$g^{(3)}(x) = \frac{\langle I_j(x) I_j(0) I_j(-x) \rangle}{I(x) I(0) I(-x)}, \quad (5)$$

$$g^{(4)}(x) = \frac{\langle I_j(x) I_j(0) I_j(-x) I_j(-2x) \rangle}{I(x) I(0) I(-x) I(-2x)}. \quad (6)$$

Note that the arguments of intensities used in (5), (6) are chosen so as to provide the maximal visibility. In the above-described coincidence method of $g^{(3)}$ measurement, this was achieved by scanning two detectors in opposite directions and the third one being fixed; for a $g^{(4)}$ measurement, the fourth detector should be scanned with a double speed.

Fig.5 shows the third-order (a) and fourth-order (b) interference patterns obtained for coherent sources by means of digital-image processing. For convenience and similarity with Fig.3, the x coordinate, originally measured in pixels, is plotted in phase units, so that $x = \phi_{12}$; the other phases obey the relations $\phi_{32} = -\phi_{12}$, $\phi_{42} = -2\phi_{12}$. As expected, the distribution in Fig 5a is similar to the third-order interference pattern registered by means of coincidence method. The interference visibilities achieved for three- and four-photon interference are 73% and 93%, respectively. For comparison, theoretical dependencies given by Eqs (2), (3) are shown as thin solid lines. The averaged distribution of the intensity (shown in both plots by empty circles) has almost no modulation with the period of the interference pattern; the observed non-uniformity is caused by the interference pattern envelope and the edge effects in the EOM.

Similar dependencies (with smaller visibilities) were measured for the case of pseudo-thermal sources.

In conclusion, we have demonstrated, both theoretically and experimentally, that while the classical visibility limit for two-photon interference is only 50%, it becomes considerably higher in the multi-photon case. Three-photon and four-photon interference has been observed both for coherent and pseudo-thermal light, and the maximal visibility values 74% and 93% have been achieved. These results, on the one hand, show that classical pulsed radiation, in addition to the high spatial resolution of ghost diffraction and ghost imaging, can also provide a high visibility, but in this case multi-photon correlations should be used. On the other hand, our results establish a visibility 'threshold' in multi-photon interference experiments: for the interference to be clearly nonclassical, the visibility should exceed 81.9% in the three-photon case and 94.4% in the four-photon one. Since exceeding these rather high values is practically difficult, we suggest that the visibility criterion should be simply avoided in multi-photon interference experiments, and some other observable signs of nonclassicality be used, such as the Lee-Klyshko criterion [18], relations between the different-order normalized ICFs [14], or the scaling of normalized ICFs with the mean photon number [19]. This work was supported in part by the RFBR grants # 06-02-16393, # 05-02-16391, # 06-02-39015-GFEN and the Program of Leading Scientific Schools Support, # NSh-4586.2006.2. T.Sh.I. acknowledges the support of the 'Dynasty' Foundation.

-
- [1] R. Ghosh and L. Mandel, Phys. Rev. Lett. 59, 1903 (1987).
 - [2] D. V. Strekalov, A. V. Sergienko, D. N. Klyshko, and Y. H. Shih, Phys. Rev. Lett. 74, 3600-3603 (1995)
 - [3] T. B. Pittman, Y. H. Shih, D. V. Strekalov, and A. V. Sergienko, Phys. Rev. A 52, R3429-R3432 (1995)
 - [4] R. Hanbury Brown and R. Q. Twiss, Nature, 178, 1046-1048 (1956).
 - [5] A. B. Haner and N. R. Isenor, American Journal of Physics, 38, 6, P. 748-751 (1970).
 - [6] Y.-H. Zhai, X.-H. Chen, D. Zhang, and L.-A. Wu, Phys. Rev. A 72, 043805 (2005).
 - [7] R. I. Pfleegor and L. Mandel, Phys. Rev. 159, 1084-1088 (1967); Z. Y. Ou, E. C. Gage, B. E. Magill, and L. Mandel, Optics Communications, 69 (1), 1-5 (1988).
 - [8] A. Gatti, E. Brambilla, M. Bache, and L. A. Lugiato, Phys. Rev. Lett. 93, 093620 (2004); F. Ferri, D. Magatti, A. Gatti, M. Bache, E. Brambilla, and L. A. Lugiato, Phys. Rev. Lett. 94, 183602 (2005).
 - [9] R. S. Bennink, S. J. Bentley, and R. W. Boyd, Phys. Rev. Lett. 89, 113601 (2002).
 - [10] G. Scarcelli, A. Valencia, and Y. Shih, Phys. Rev. A 70, 051802(R) (2004); M. DAngelo, A. Valencia, M. H. Rubin, and Y. Shih, Phys. Rev. A 72, 013810 (2005).
 - [11] R. Glauber, Phys. Rev. 130, 2529 (1963).
 - [12] L. Mandel, Phys. Rev. A 28, 929-943 (1983).

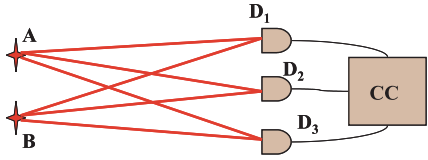


FIG. 1: Observation of three-photon interference in the Young double-slit scheme.

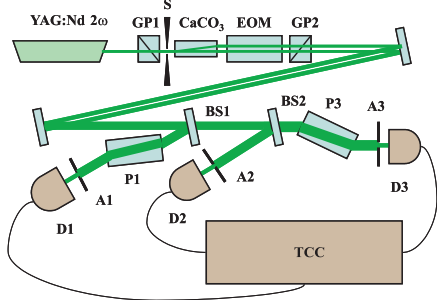


FIG. 2: Experimental setup. GP1 and GP2, Glan prisms; S, a slit; EOM, electro-optic modulator; BS1, 33%/67% beam-splitter; BS2, 50% beamsplitter; A1-3, apertures; P1,3, glass plates; D1-3, avalanche photodiodes; TCC, triple coincidence circuit.

- [13] D. N. Klyshko, Physics-Uspekhi, 37 (11), 1097 (1994).
- [14] D. N. Klyshko, Physics-Uspekhi, 39(6), 573 (1996).
- [15] M. W. Mitchell, J. S. Lundeen, and A. M. Steinberg, Nature 429, 161-164 (2004); Ph. Walther, J.-W. Pan, M. Aspelmeyer, R. Ursin, S. Gasparoni, and A. Zeilinger, Nature 429, 158-161 (2004); Zh. Zhao, T. Yang, Y.-A. Chen, A.-N. Zhang, M. Zukowski, and J.-W. Pan, Phys. Rev. Lett. 91, No 18, 180401 (2003).
- [16] Description of other types of two-beam interferometers such as, for instance, Mach-Zehnder one, is similar.
- [17] M. Bache, D. Magatti, F. Ferri, A. Gatti, E. Brambilla, and L. A. Lugiato, Phys. Rev. A 73, 053802 (2006).
- [18] E. Waks, B. C. Sanders, E. Diamanti, and Y. Yamamoto, Phys. Rev. A 73, 033814 (2006).
- [19] O. A. Ivanova, T. Sh. Iskhakov, A. N. Penin, M. V. Chekhova, Quantum Electronics 36 (10) 951 - 956 (2006).

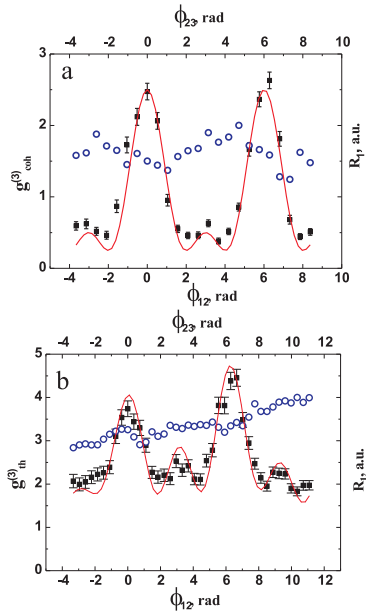


FIG. 3: Interference pattern in the normalized third-order ICF for (a) coherent sources (b) pseudo-thermal sources obtained by tilting glass plates at the inputs of detectors 1 and 3. Empty circles show the intensity distribution given by the counting rate R_1 of detector 1. Solid lines show the theoretical fit with Eq.(2)

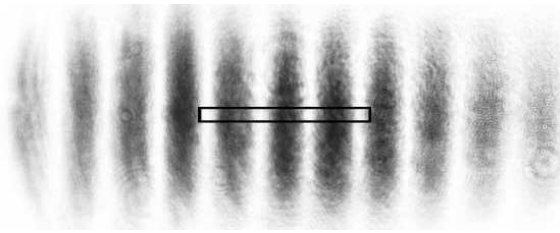


FIG. 4: Single-pulse photograph of the Young interference pattern for two coherent sources. The rectangle shows the dimensions of the processed area.

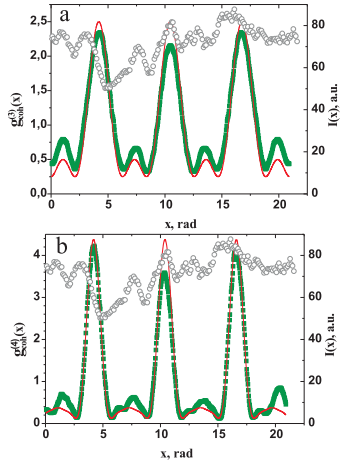


FIG. 5: Interference patterns in normalized third-order (a) and fourth-order (b) ICFs for coherent sources obtained by processing digital images as shown in Fig.4. The averaged intensity distribution in the x coordinate is shown in both plots by empty circles. Thin solid lines show the theoretical dependencies (2) (Fig.5a) and (3) (Fig.5b).